International Journal of Materials Science
ISSN 0973-4589 Volume 12, Number 3 (2017), pp. 433-442

http://www.ripublication.com

Structural and Magnetic Properties of Cr^{3+} Substituted Nickel Zinc Copper Nano Ferrites

B. L. Shinde[1], V. S. Suryavanshi [2] and K. S. Lohar [3*]

[1] Department of Chemistry, Waghire College, Saswad Dist: Pune, 412301 (M.S.) India

[2] Department of Chemistry, Shri Chatrapati Shivaji College, Omerga, Dist: Osmanabad 413 613 (M.S.) India

[3] Department of Chemistry, Shrikrishna Mahavidyalaya, Gunjoti, 413606, Dist: Osmanabad (M.S.) India

**Corresponding author*

Abstract

Cr^{3+} substituted nickel zinc copper ferrites with composition $Ni_{0.2}Cu_{0.2}Zn_{0.6}Fe_{2-x}Cr_xO_4$ **(**x = 0.0, 0.2, 0.4, 0.6, 0.8 and 1.0) were synthesized by sol-gel auto combustion method. Sintering temperature of precursors was determined from TGA-DTA. XRD studies indicated that all samples possess single cubic spinel structure. Lattice constant and crystalline size of samples was decreases with increasing Cr^{3+} concentration. IR high frequency bands ($\nu_1 \approx 600$ cm^{-1}) assigned to the tetrahedral and low frequency bands ($\nu_2 \approx 450$ cm^{-1}) assigned to the octahedral complex. The microstructures of the prepared samples were studied by SEM and TEM. Remanant magnetization of NiCuZn ferrite decreased with the substitution of Cr^{3+}.

Keywords: TGA/DTA, Transmission Electron Microscopy, Remanant magnetization.

1. INTRODUCTION:

Nano spinel ferrites have been widely studied in recent years for their useful electrical, dielectric and magnetic properties and applications in information storage systems, magnetic bulk cores, magnetic fluids, microwave absorbers and high frequency devices [1]. The magnetic behavior of fine-particles is of considerable interest both from scientific and practical point of view [2]. In nano particles, the saturation magnetization (M_S), magneto crystalline anisotropy (K), curie temperature (T_C) and coercivity (H_C) values are found to differ from their bulk behavior [3]. The NiCuZn spinel ferrites are soft magnetic materials, which have large applications in advanced technologies such as multilayer chip inductors (MLCIs), multilayer LC filters [4], and magnetic temperature sensors [5]. The NiCuZn spinel ferrites have potential applications in biomedicine [6], magnetic drug delivery and cell- sorting system [7]. Several studies have focused their concentration on NiCuZn spinel ferrites since copper containing ferrites have attractive electrical and magnetic properties. In this study we report the synthesis of Cr^{3+} substituted nickel zinc copper ferrites adopting the sol gel auto combustion method and their structural and magnetic properties.

2. EXPERIMENTAL

Material and *Synthesis*

Nano Cr^{3+} substituted nickel zinc copper spinel ferrites, with composition of $Ni_{0.2}Cu_{0.2}Zn_{0.6}Fe_{2-x}Cr_xO_4$ **(**x = 0.0, 0.2, 0.4, 0.6, 0.8 and 1.0) were synthesized by the sol-gel auto-combustion method. Analytical reagent grade nickel nitrate, copper nitrate, zinc nitrate, chromium nitrate and iron nitrate in stichiometric proportion were dissolved in distilled water. The molar ratio of metal nitrates to citric acid was 1:3. An aqueous solution of citric acid was mixed with the metal-nitrate solution, and ammonia solution was slowly added to adjust the pH ≈ 7. The mixed solution was placed on a hot plate with continuous stirring at 90 °C. During evaporation, the a very viscous brown gel, which after evaporation of began to froth and ignited and burnt with glowing flints yielding brown-colored precursor. Sintering temperature is determined from TGA / DTA and prepared powders of all the precursor samples were sintered at 500 °C for 4 h to obtain the final product.

Characterization

Thermo gravimetric (TG) and differential thermal analysis (DTA) of precursors were carried on SDT Q600 V20.9 Build 20 instrument in air atmosphere at heating rate 10^0 C / min. X-ray powder diffraction with Cu-K_α radiation (λ=1.5405 Å) by Phillips X-ray diffractometer (Model 3710). The infrared spectra recorded at room temperature

in the range 200 to 800 cm^{-1} using Perkin Elmer infrared spectrophotometer. Morphology and structure of the powder samples were studied on JEOL-JSM-5600 N Scanning Electron Microscope (SEM) and on Philips (model CM 200) Transmission Electron Microscope (TEM). The magnetic measurements were performed at room temperature using a commercial PARC EG&G VSM 4500 vibrating sample magnetometer.

3. RESULTS AND DISCUSSION

Thermal Analysis (TGA / DTA)

Figure 1 Typical TGA/DTA plot for Cr^{3+} substituted ferrite (x=1.0) illustrates first around 80 ^oC dehydration takes place with endothermic peak in DTA. Then around 360 ^oC decomposition of unreacted citric acid observed with evolution of heat indicated by exothermic peak, forming spinel ferrite.

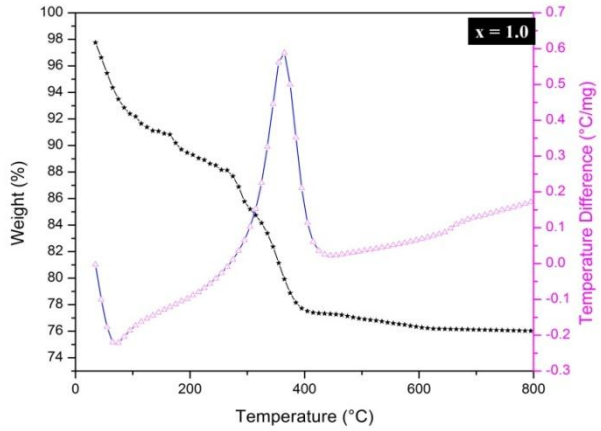

Figure 1: TGA-DTA plot for precursor of $Ni_{0.2}Cu_{0.2}Zn_{0.6}Fe_{2-x}Cr_xO_4$ (x = 1.0)

Therefore, the synthesized powders of all the samples were sintered at 500 °C for 4 hour to obtain the final product.

X-ray diffraction

Typical X-ray diffraction (XRD) patterns of the $Ni_{0.2}Cu_{0.2}Zn_{0.6}Fe_{2-x}Cr_xO_4$ spinel ferrite system with x = 0.0 and 0.6, are shown in Figure 2.

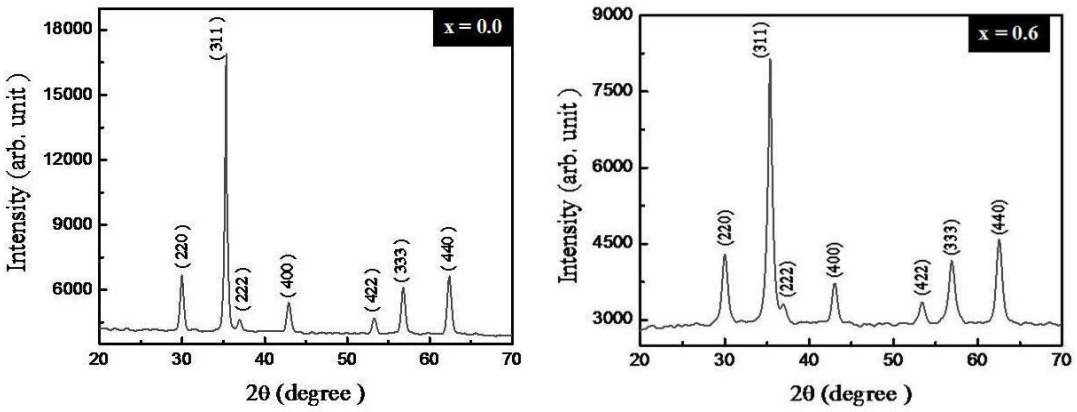

Figure 2: XRD patterns for samples x =0.0 and x=0.6

The XRD patterns confirmed the formation of cubic spinel structure of single phase ferrites.

Lattice parameter (a) of all the samples was determined by using the following equation [8]:

$$a = d\sqrt{h^2 + k^2 + l^2} \qquad (1)$$

Lattice constant values were calculated for each sample using XRD pattern Figure 3 shows the variation of lattice constant with Cr^{3+} substitution.

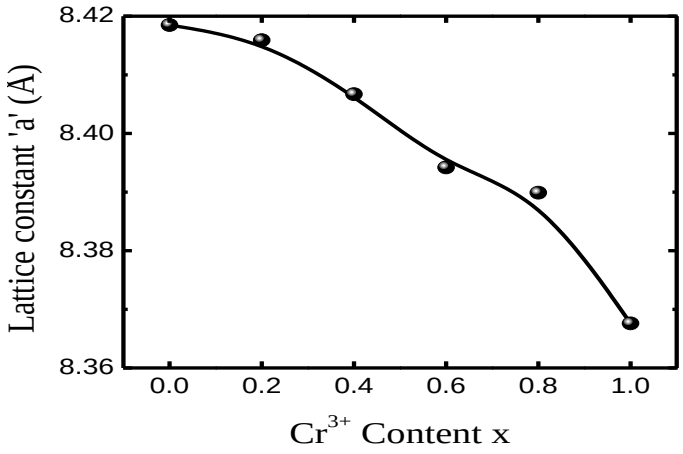

Figure 3: Variation of experimental lattice constant with Cr^{3+} substitution of $Cu_{0.2}Ni_{0.2}Zn_{0.6}Fe_{2-x}Cr_xO_4$.

The X-ray density of all the samples was obtained by the following relation:

$$d_x = \frac{8M}{Na^3} \qquad (2)$$

Where, 8 is formula unit, M is molecular weight, N is Avogadro's number, a is lattice constant. The values of X-ray density are presented in Figure 4. It is observed from Figure 4 that like lattice parameter, X-ray density also decreased with increasing Cr^{3+} content x.

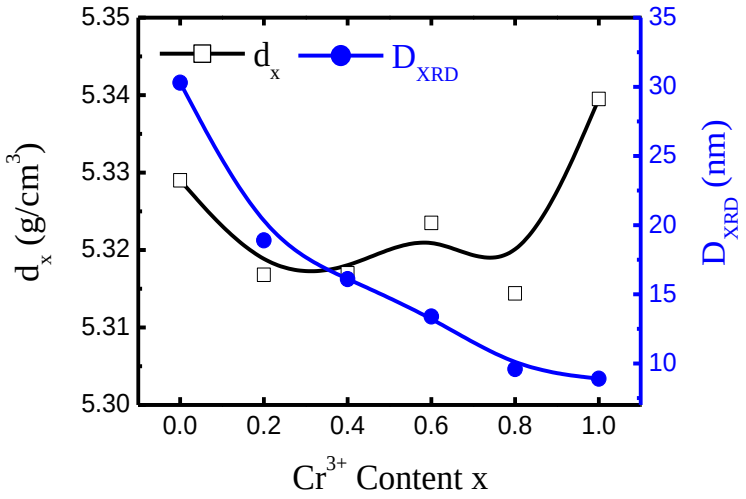

Figure 4: Variation of x-ray density and crystallite size with Cr^{3+} substitution of $Ni_{0.2}Cu_{0.2}Zn_{0.6}Fe_{2-x}Cr_xO_4$.

The average crystallite diameter 'D_{XRD}' of powder estimated from the most intense (311) peak of XRD and using the Debye-Scherrer method [8]:

$$D_{XRD} = \frac{C\lambda}{B_{1/2}\cos\theta} \qquad (3)$$

Where, $B_{1/2}$ is the full width of half maximum in (2θ), θ is the corresponding Bragg angle and C = 0.9. The variation of the crystallite size with Cr^{3+} substitution is shown in Figure 4. The crystallite size is decreases from 30.3 nm to 8.9 nm with increasing Cr^{3+} substitution.

Infrared spectroscopy

Figure 5 represents typical IR spectra (x= 0.0 and x = 1.0. It is observed from figure that the higher frequency band (ν_1) is appeared in the range of 568 - 611 cm^{-1} assigned to tetrahedral site whereas lower frequency band (ν_2) is appeared in the range of 388 - 492 cm^{-1} assigned to octahedral site. These bands are characteristics features of spinel structure. It explains that the normal mode of vibration of tetrahedral cluster is higher than that of octahedral cluster. It should be attributed to the shorter bond length of tetrahedral cluster and longer bond length of octahedral cluster [9].

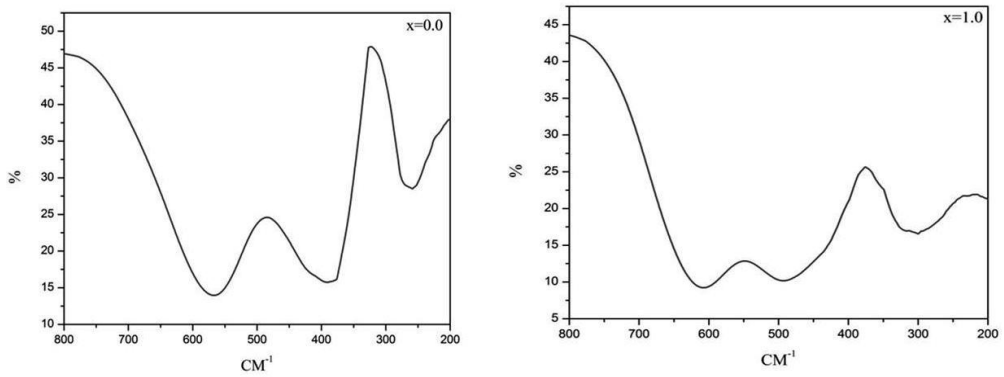

Figure 5: IR spectra for the sample x=0.0 and x=0.6 of the series

Scanning electron microscopy (SEM)

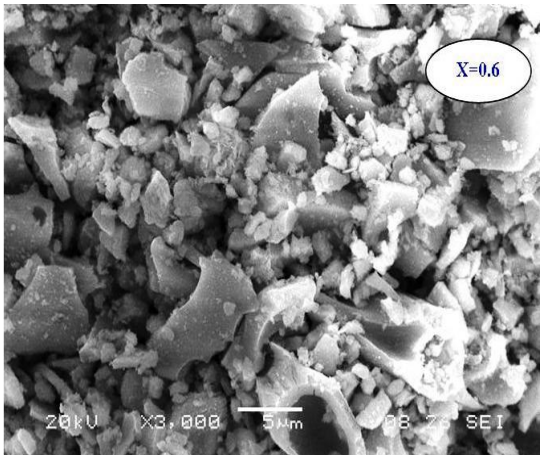

Figure 6: Scanning electron micrograph for sample x = 0.6

Typical Scanning electron micrographs (SEM) of the surfaces of the sample x = 0.6 is shown in Figure 6. It is observed from the SEM images that the prepared samples are amorphous and porous in nature.

Transmission Electron Microscopy (TEM)

TEM image and particles size distributions of the typical sample x = 0.0 is presented in Figure 7. The particles were well distributed with a little agglomeration. The agglomeration is the indication of high reactivity of the prepared sample with the heat treatment and it may also be come from the magnetostatic interaction between particles.

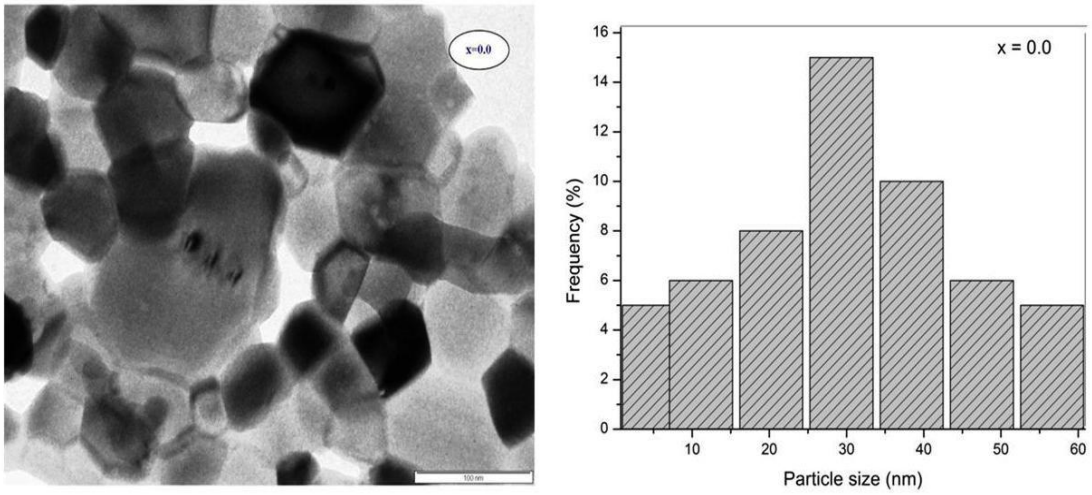

Figure 7: Transmission electron micrograph and Particle size distribution for sample x = 0.6

Nanocrystalline particles observed were in the range 6-55 nm. Particles with size between 10-35 nm were most abundant (more than 70%)

Magnetization

Figure 9 shows the hysteresis loops of all the samples of $Ni_{0.2}Cu_{0.2}Zn_{0.6}Fe_{2-x}Cr_xO_4$. It is observed from the hysteresis loops that, all compositions analyzed produced narrow loops, with a behavior characteristic of soft magnetic materials (easy magnetization and demagnetization).

Observed (n_B Obs.) and calculated (n_B Cal.) magnetic moments were determined using the following equations [10, 11]:

$$n_B\ obs. = \frac{Molecular\ weight\ \times\ saturation\ magnetization}{5585} \qquad (14)$$

$$n_B\ Cal. = M_B - M_A \qquad (15)$$

where, M_B and M_A are the B and A sub-lattice magnetic moments in μ_B.

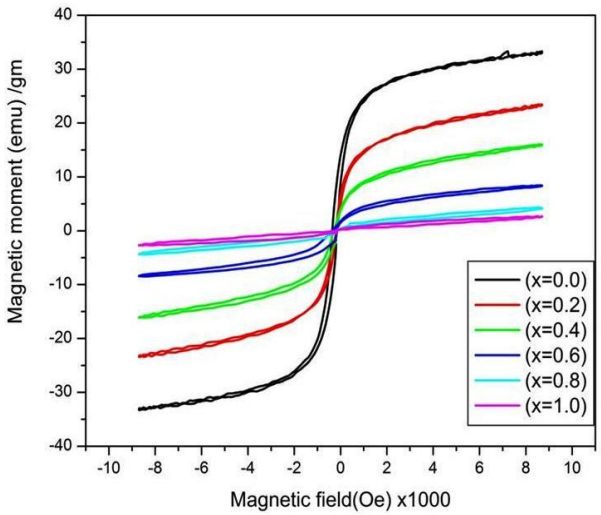

Figure 8: Hysteresis loops for $Cu_{0.2}Ni_{0.2}Zn_{0.6}Fe_{2-x}Cr_xO_4$

Table 1: Magnetization saturation (M_s), Remanant magnetization (Mr) and magneton number (n_B) of system $Cu_{0.2}Ni_{0.2}Zn_{0.6}Fe_{2-x}Cr_xO_4$

Composition	Mr	(Ms)	(n_B)	
'x'	(emu/g)	(emu/g)	Obs.	Cal.
0.0	14.0	32.8	1.406	8.016
0.2	8.4	24.1	1.030	7.606
0.4	4.5	15.9	0.677	7.196
0.6	2.2	8.3	0.352	6.786
0.8	0.9	4.1	0.173	6.376
1.0	0.7	2.7	0.114	5.966

It is observed from Table: 1 that the saturation magnetization (Ms), Remanant magnetization (Mr) of NiCuZn ferrite decreased with the substitution of Cr^{3+} ions.

It is well known that Cr^{3+} ion has a strong octahedral site preference and lower magnetic moment compared with that of Fe^{3+} ions. It is observed from cation distribution data that Cr^{3+} ion has a strong octahedral site preference and lower magnetic moment ($3\mu_B$) compared with that of Fe^{3+} ions ($5\mu_B$). The observed decrease in magnetic field at B site with increase in Cr^{3+} content is attributed to the dilution of the field component from Fe^{3+} ions in neighboring B site, which decreases the A–B exchange interactions and results in decrease in the magnetization. The magnetic

moments calculated from Neel's molecular field model decreased with Cr^{3+} substitution (Table: 1) and are in agreement in the experiment results suggesting that the structure remain collinear with increasing Cr^{3+} substitution. Further, the tetrahedral and octahedral sublattices of ferrite may be subdivided such that the resultant vectors of the magnetic moments of the sublattices are aligned in such a direction that will influence the effective magnetization. Thus, the decrease in Ms may be explained by the formation of a collinear spin arrangement due to the Cr^{3+} substitution.

CONCLUSION

TGA shows two weight loss steps corresponding to endothermic and exothermic DTA peaks. XRD studies illustrates that all samples possess single cubic spinel structure. Lattice constant decreases from 8.418 Å to 8.367 Å and crystalline size of samples was decreases from 30.3 to 8.9 nm with increasing Cr^{3+} concentration. IR higher frequency band (ν_1) is appeared in the range of 568 - 611 cm^{-1} assigned to tetrahedral site whereas lower frequency band (ν_2) is appeared in the range of 388 - 492 cm^{-1} assigned to octahedral site. Nanocrystalline particles observed were in the range 6-55 nm. Particles with size between 10-35 nm were most abundant (more than 70%). The SEM and TEM illustrates that samples are amorphous and porous in nature. Saturation magnetization (Ms), Remanant magnetization (Mr) of NiCuZn ferrite decreased with the substitution of Cr^{3+} ions.

REFERENCES:

[1] Chand, Jagdish, et al. "Effect of Gd^{3+} doping on magnetic, electric and dielectric properties of $MgGd_xFe_{2-x}O_4$ ferrites processed by solid state reaction technique." *Journal of Alloys and Compounds* 509.40 (2011): 9638-9644.

[2] H. J. Richter, "Recent advances in the recording physics of thin-film media" J. Phys. D : *Appl. Phys*., 32 (1999) R-147.

[3] Panda, R. N., and N. S. Gajbhiye. "Magnetic properties of single domain ε-Fe3N synthesized by borohydride reduction route." *Journal of applied physics* 81.1 (1997): 335-339.

[4] Su, Hua, et al. "Sintering characteristics and magnetic properties of NiCuZn ferrites for MLCI applications." *Materials Science and Engineering: B* 129.1 (2006): 172-175.

[5] Hossain, AKM Akther, and M. L. Rahman. "Enhancement of microstructure and initial permeability due to Cu substitution in $Ni_{0.50-x}Cu_xZ_{0.50}Fe_2O_4$.

ferrites." *Journal of Magnetism and Magnetic Materials* 323.15 (2011): 1954-1962.

[6] He, Y. P., et al. "Synthesis and characterization of functionalized silica-coated Fe3O4 superparamagnetic nanocrystals for biological applications." *Journal of Physics D: Applied Physics* 38.9 (2005): 1342.

[7] Pope, Niedre M., et al. "Evaluation of magnetic alginate beads as a solid support for positive selection of CD34+ cells." *Journal of Biomedical Materials Research Part A* 28.4 (1994): 449-457.

[8] B. D. Cullity, *"Elements of X-ray diffraction",* (Addison-Wesley Publ. Comp. Inc., Reading, Massachusetts, U.S.A.) (1956), 99.

[9] Hemeda, O. M., et al. "Effect of sintering on X-Ray and IR spectral behaviour of the MnAlxFe2-xO4 ferrite system." *physica status solidi (a)* 156.1 (1996): 29-38.

[10] K.J. Standley, *Oxide magnetic materials*, (Clarendon Press, Oxford, 1972)

[11] Neel, Ls. "Magnetic properties of ferrites: ferrimagnetism and antiferromagnetism." *Ann. Phys* 3 (1948): 137-198.